

BARYON FORM FACTORS AT HIGH MOMENTUM TRANSFER AND GPD'S

PAUL STOLER

Physics Department, Rensselaer Polytechnic Institute, Troy NY12180

Nucleon elastic and transition form factors at high momentum transfer $-t$ are treated in terms of generalized parton distributions in a two-body framework. In this framework the high $-t$ dependence of the form factors give information about the high k_{\perp} , or short distance b_{\perp} correlations of nucleon model wave functions. Applications are made to elastic and resonance nucleon form factors, and real Compton Scattering.

During the past several years there has been considerable discussion of how to describe exclusive reactions at momentum transfers which are experimentally attainable. While pQCD is an interesting mechanism which probes the simplest Fock state component of the hadron, most theoretical studies agree that even at the highest attainable momentum transfers, there is a large *soft* contribution which involves more complex components of the hadronic wave functions. The so-called handbag ¹ mechanism has evolved to describe such soft processes, and achieves its full power at high momentum transfer where a process can be factorized into a fully perturbative hard amplitude and a *generalized parton distribution* (GPD) ^{2 3 4}, which represents the off-diagonal probability of the interacting quark being placed back into the remaining hadron, keeping it in-tact at a different transferred longitudinal momentum. The power of the mechanism is that the same soft GPD, which contains the information about the hadronic structure is accessed in a variety of different reactions, while the hard perturbative part is reaction specific. The GPD's give us unique information about the longitudinal (x) and transverse (k_{\perp}) parton momentum distributions, and importantly, about the interference between the initial parton wave function and the phase shifted final parton wave function.

The GPD approach manifests itself in two kinematical regimes, corresponding to the t dependent *form factor* type reaction, and the $t \rightarrow t_{min}$ *off-forward* production of mesons or photons. Here we focus on the former. In such a reaction the incident real or virtual photon interacts perturba-

tively with one of the quarks within the hadron, which is re-absorbed into the hadron leaving it in-tact or in a higher resonant state. This is a Feynman type reaction which involves the full complexity of the non-perturbative nucleon structure, as opposed to the leading order pQCD mechanism, which involves only the valence quark Fock state. Form factors are the x moments of the GPD's, and as such constrain the longitudinal dependence of the nucleon structure. As a function of t they uniquely constrain the k_\perp dependence of the nucleon's wave functions. Fourier transforms of the GPD's - $\mathcal{F}_b(x, \vec{b}_\perp) \propto \int d\vec{q}_\perp \exp(i\vec{b}_\perp \cdot \vec{q}_\perp) \mathcal{F}(x, t)$ -, directly give the transverse spatial impact parameter distribution of the quarks for each longitudinal momentum fraction ⁵. Thus, together with x distributions obtained in DIS the k_\perp accessed in form factor measurements give us a unique 3 dimensional picture of the quark distributions in the nucleon. Examples of reactions accessible via GPDs include the nucleon elastic Dirac and Pauli form factors F_1 and F_2 (or equivalently G_{Ep} and G_{Mp}), resonance transition amplitudes such as $A_{1/2}$ for $N \rightarrow S_{11}(1535)$, or G_M^* for $N \rightarrow \Delta$, and Compton scattering form factors R_V and R_A and their polarization asymmetries. The relationship of the GPD's to these various form factors is given as follows:

For elastic scattering

$$F_1(t) = \int_0^1 \sum_q \mathcal{F}^q(x, t) dx \quad F_2(t) = \int_0^1 \sum_q \mathcal{K}^q(x, t) dx. \quad (1)$$

where q signifies both quark and anti-quark flavors. We work in a reference frame in which the total momentum transfer is transverse so that $\zeta=0$, and denote $\mathcal{F}^q(x, t) \equiv \mathcal{F}_0^q(x, t)$, $\mathcal{K}^q(x, t) \equiv \mathcal{K}_0^q(x, t)$.

For Compton scattering ⁶

$$R_1(t) = \int_0^1 \sum_q \frac{1}{x} \mathcal{F}^q(x, t) dx \quad R_2(t) = \int_0^1 \sum_q \frac{1}{x} \mathcal{K}^q(x, t) dx. \quad (2)$$

Resonance transition form factors access components of the GPD's which are not accessed in elastic scattering or Compton scattering. The $N \rightarrow \Delta$ form factors are related to isovector components of the GPD's ^{7 8}.

$$G_M^* = \int_0^1 \sum_q \mathcal{F}_M^q(x, t) dx \quad G_E^* = \int_0^1 \sum_q \mathcal{F}_E^q(x, t) dx \quad G_C^* = \int_0^1 \sum_q \mathcal{F}_C^q(x, t) dx \quad (3)$$

where G_M^* , G_E^* and G_C^* are magnetic, electric and Coulomb transition form factors ⁹, and \mathcal{F}_M^q , \mathcal{F}_E^q , and \mathcal{F}_C^q are axial (isovector) GPD's, which can be related to elastic GPD's in the large N_C limit through isospin rotations ⁸. The $N \rightarrow S_{11}$ transition form factor is also important, as it probes fundamental aspects of dynamical chiral symmetry breaking in QCD. If chiral

symmetry were not broken, the S_{11} would be the nucleon's parity partner and the N and S_{11} masses would be degenerate.

As a basis for constructing the GPD's we use the two-body model introduced in ⁶ whose connection with the handbag is illustrated in fig. 1.

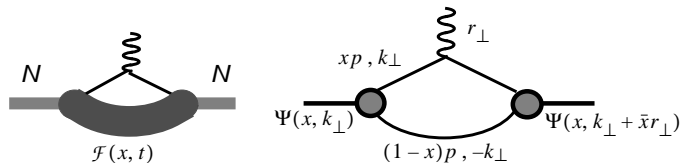


Figure 1. Schematic relation between the two-body and handbag mechanisms discussed in the text.

In this framework the GPD is written

$$\mathcal{F}(x, t) = \int \Psi^*(x, k_\perp + \bar{x}r_\perp) \Psi(x, k_\perp) \frac{d^2 k_\perp}{16\pi^3} \quad (4)$$

where $\bar{x} \equiv 1 - x$,

An example of a specific model wave function ¹⁰ is

$$\Psi(x, k_\perp) = \Phi(x) \left(A_s e^{-k_\perp^2/2x\bar{x}\lambda^2} + A_h \frac{x\bar{x}\Lambda^2}{k_\perp^2 + \Lambda^2} \right) \equiv \Psi_{soft} + \Psi_{hard} \quad (5)$$

The function $\Phi(x)$ is constrained so that $\mathcal{F}(x, 0)$ reduces to the valence quark distribution $f(x)$. It was shown in ref. ¹⁰ that although a Gaussian form of the k_\perp dependence in Ψ_{soft} accounts for the magnitude and shape of the elastic F_1 for Q^2 below several GeV^2 , it is inadequate at higher Q^2 . However, the addition of a small Ψ_{hard} component in eq. (5) can dramatically improve the agreement at high Q^2 . As an example of a power law dependence, we choose an *ad-hoc* $1/k_\perp^2$ behavior with lower cutoff parameter Λ . A similar parameterization is chosen for F_2 with $\mathcal{K}^q(x, 0) = \sqrt{(1-x)}\mathcal{F}^q(x, 0)$. In order to constrain the parameters of eq. (5) the available data on both G_{Mp} and G_{Ep}/G_{Mp} were simultaneously reproduced, giving $A_s = \sqrt{1 - A_h^2} = 0.97$, $A_h = 0.24$, $\lambda_1^2 = 0.6 \text{ GeV}^2$ and $\lambda_2^2 = 0.45 \text{ GeV}^2$. The function $\Psi(k_\perp) = \int \Psi(k_\perp, x) dx$ is shown in fig. 2. Only at k_\perp greater than about 1 GeV does the hard tail important.

The fits to the data using respectively $\Psi = \Psi_{soft} + \Psi_{hard}$, and $\Psi = \Psi_{soft}$ are shown in figs. 3 4 6.

As seen in the top panel of fig. 3, this rather small addition of high momentum components can account for the high, as well as the low Q^2 magnetic form factor. Interestingly, ref. ¹¹ found that even in a pQCD calculation a power law tail is useful in reproducing the high Q^2 data.

Figure 2. The function $\Psi(k_\perp) \equiv \int \Psi(x, k_\perp) dx$ vs. k_\perp . The dashed curve is due to the soft Gaussian component Ψ_{soft} , with $\lambda^2 = 0.6 \text{ GeV}^2$. The solid curve is $\Psi_{soft} + \Psi_{hard}$, with $A_h = 0.24$, $k_{\perp, max} = 4 \text{ GeV}$, and cutoff parameter $\Lambda = 0.45 \text{ GeV}$.

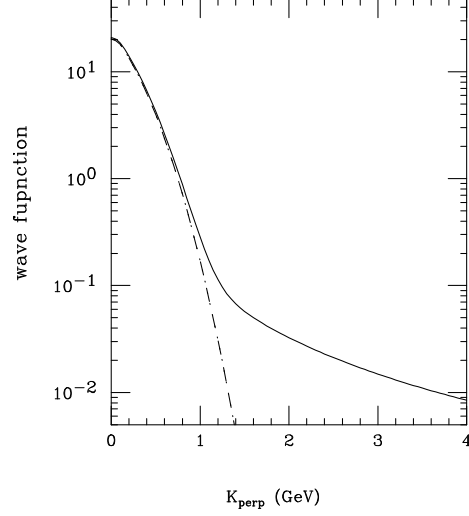
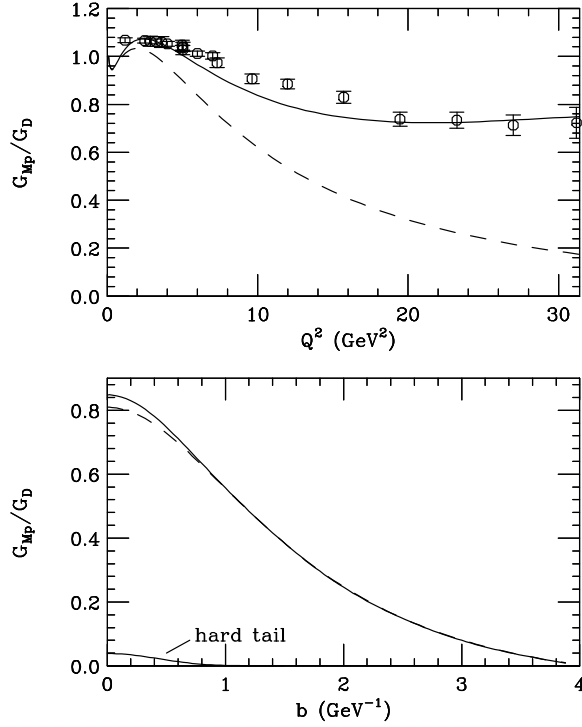


Figure 3. Upper: Proton magnetic form factor G_{Mp}/G_D , where $G_D = 1/(1 + Q^2/0.71)^2$. Data are from SLAC^{9,10} with low energy data reevaluated¹¹. The dashed curve uses only Ψ_{soft} , while the solid curve uses $\Psi_{soft} + \Psi_{hard}$. Lower: The impact parameter dependence of the curves in the upper figure, $G_{Mp}(b_\perp) = \int dx \mathcal{F}_b(x, b_\perp)$. The curve at the bottom left labelled "hard tail" is the difference between the solid and dashed curves, which is responsible for most of the form factor at high Q^2 .



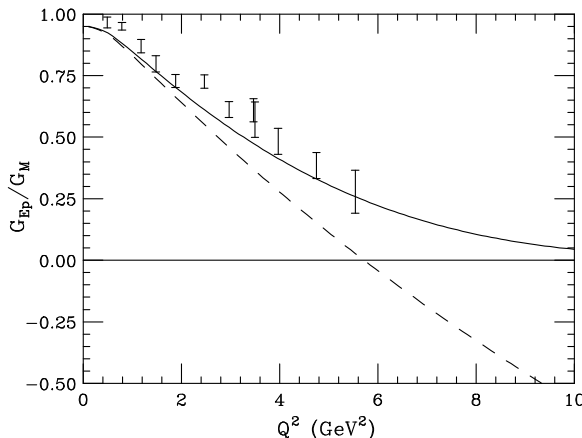
Taking the Fourier transforms of the GPD's gives the spatial impact parameter distribution of the struck quarks. The bottom panel in fig. 3 shows

$$\mathcal{F}_b(x, b_\perp) = \int dq_\perp e^{i\vec{b}_\perp \cdot \vec{q}_\perp} \mathcal{F}(x, t).$$

and the effect of Ψ_{hard} . Only a small addition of small impact parameter components to the wave function accounts for most of the form factor at high Q^2 .

In fig. 4 the obtained values of GE_p/GM_p for $\Psi_{soft} + \Psi_{hard}$ and Ψ_{hard} alone are compared with the recent JLab data¹².

Figure 4.
 GE_p/GM_p for $\Psi_{soft} + \Psi_{hard}$ and Ψ_{hard} alone are compared with the recent JLab data¹². The curves are as in fig. 3.



The obtained GPD's as a function of x and t are shown in fig. 5.

One may apply the constraints of the elastic form factors to investigate properties of inelastic resonance transitions. For example, in the large N_c limit the GPDs for the $N \rightarrow \Delta(1232)$ transition are expected to be isovector components of the elastic GPD, which is approximately given by

$$\mathcal{F}_M^{(IV)} = \frac{2}{\sqrt{3}} \mathcal{K}_M^{(IV)} = \frac{2}{\sqrt{3}} (\mathcal{K}^u - \mathcal{K}^d),$$

where \mathcal{K}^u and \mathcal{K}^d are the GPD's for the up and down quarks respectively. Figure 6 shows the result of applying the GPD's from elastic scattering to the $N \rightarrow \Delta$ transition. The data was renormalized by the ratio 3/2.14, to bring into line the nucleon isovector form factor at $Q^2=0$ with the experimental value for the $N \rightarrow \Delta$.

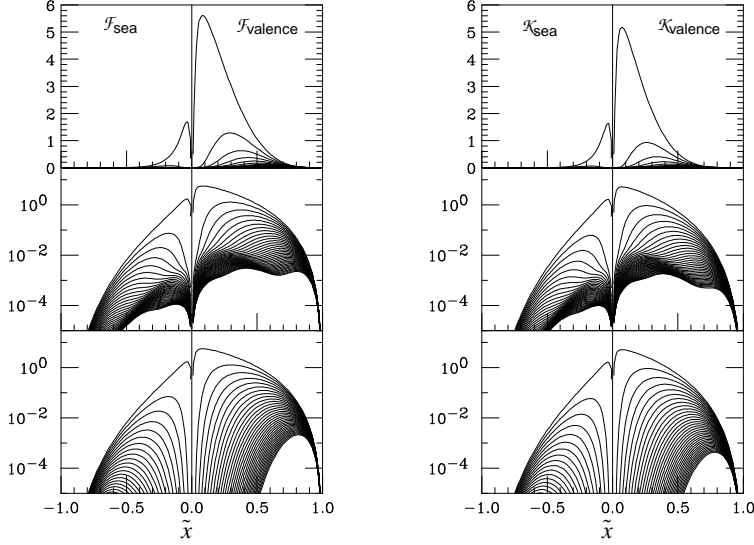


Figure 5. GPD's as a function of \tilde{x} for various values of t , where $\tilde{x} = x$ (x-tilde) for valence quarks, and $\tilde{x} = -x$ for the sea quarks. The figures on the left and right are for \mathcal{F} and \mathcal{K} respectively. The graphs for positive \tilde{x} represent the *valence* quark contribution, while the graphs for negative \tilde{x} represent the *sea* quark contributions. The individual curves range from $|t| \sim 0 \text{ GeV}^2$ (highest curve in each panel) to $|t| = 35 \text{ GeV}^2$ (lowest curve in each panel). The upper and middle panels are the GPD's for the full wave function $\Psi_{soft} + \Psi_{hard}$, while those in the lowest panels are obtained using the Ψ_{soft} soft only. Note that the addition of the Ψ_{hard} mainly affects the GPD's at higher $|t|$ and $\tilde{x} < 0.5$

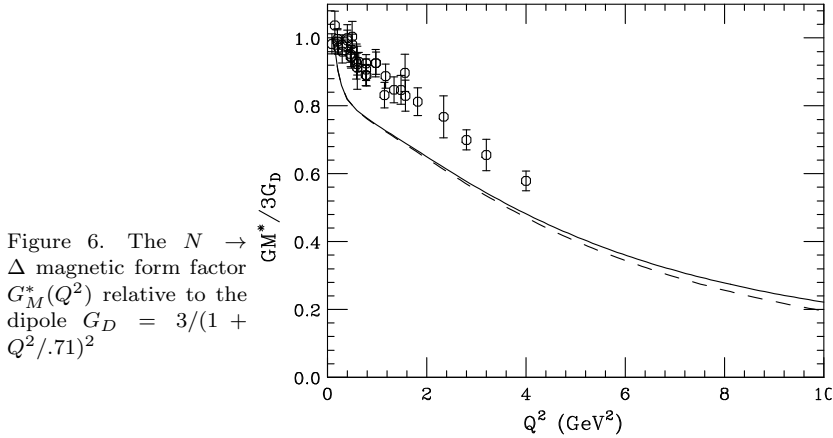


Figure 6. The $N \rightarrow \Delta$ magnetic form factor $G_M^*(Q^2)$ relative to the dipole $G_D = 3/(1 + Q^2/.71)^2$

In summary, it is seen that complete knowledge of the various types of baryon form factors provides very strong constraints for model wave

functions and GPD's.

References

1. A.V. Efremov and A.V. Radyushkin, *Theor. Math. Phys.* **42**, 97 (1980)
2. X. Ji, *Phys. Rev. Lett.* **78**, 610 (1997);
3. A. Radyushkin, *Phys. Lett.* **B380**,417 (1996); *Phys. Rev.* **D56**,5524 (1997).
4. J. Collins, L. Frankfort, and M. Strikman, *Phys. Rev.*, **D56**, 2982 (1997).
5. M. Burkardt, *Phys.Rev.***D62**,071503,(2000); also hep-ph/0207047 (2002).
6. A. Radyushkin, *Phys. Rev.* **D58**,114008 (1998).
7. L.L.Frankfurt et al.,*Phys. Rev. Lett.* **84** ,2589 (2000).
8. K.Goeke, M.V. Polyakov, and M. Vanderhaeghen, *Prog.Part.Nucl.Phys.***47**, 401,2001 (2001); also preprint hep-ph/0106012.
9. H.F. Jones and M.D. Scadron, *Annals of Physics* **81**, 1 (1979).
10. P. Stoler, *Phys. Rev.* **D65**, 053013 (2002).
11. C.A. Carlson and Franz Gross, *Phys. Rev.* **D36**, 2060 (1987).
12. L. Andihavis *et al.*, *Phys. Rev.* **D50**, 5491 (1994).
13. R.G. Arnold et al., *Phys. Rev. Lett.* **57**, 174 (1986).
14. E.J. Brash et al. *Phys. Rev.* **C65**, 051001(R) (2002).
15. M.K. Jones *et al.* *Phys. Rev. Lett.* **84**,1398 (2000); O. Gayou et al. *et al.* *Phys. Rev.* **C64**,038202 (2001).